3D position sensitive CdZnTe gamma-ray spectrometers – improved performance with new ASICs

Feng Zhang* and Zhong He

Dept. of Nuclear Engineering and Radiological Sciences, Univ. of Michigan, Ann Arbor, MI 48109

ABSTRACT

A 3-dimensional position sensitive CdZnTe gamma-ray spectrometer based on VAS3.1/TAT3 ASICs was developed and tested. The 3-D CZT spectrometer employs a $1.5 \times 1.5 \times 1$ cm^3 CdZnTe crystal with 11 by 11 pixelated anodes wire-bonded to the readout electronics. The signals from the anode pixels and the cathode were both read out through the ASICs. The pixel position provides the lateral 2-D coordinates, while the third coordinate can be determined by using depth-sensing techniques. With the help of 3-D position sensitivity, the variation in weighting potential, electron trapping and material non-uniformity can be mitigated to the scale of the position resolution, estimated to be 1.27 mm $\times$ 1.27 mm $\times$ 0.2 mm. The energies and 3-D coordinates can be reconstructed for multiple interaction events from a single incident gamma ray. The third-generation ASICs – VAS3.1/TAT3 has been developed to improve the electronic noise, uniformity, linearity and stability. Energy resolution of 0.93% FWHM and 1.52% FWHM have been achieved for single-pixel events and two-pixel events, respectively, including ~4.5 keV FWHM electronic noise.

Keywords: 3-Dimentional, position sensitive, CZT, CdZnTe, spectrometer

1. INTRODUCTION

Wide band gap semiconductor detector materials, such as CdTe, CdZnTe and HgI_2, have long been of interest because of the convenience of room temperature operation, high efficiency for gamma-ray detection and potential for good energy resolution. Among them, CdZnTe has gained particular interest. However, the performance degradation due to charge trapping limited its application when large sensitive volumes are needed. Single polarity charge sensing techniques, such as coplanar grids[1] or pixelated anodes[2], had overcome the severe hole trapping problem and greatly improved the energy resolution of large volume CdZnTe detectors. However, even with single polarity charge sensing techniques and methods to compensate for electron trapping, such as relative gain[1] and depth sensing[3], the variations in electron trapping and material non-uniformity can still degrade the energy resolution.

In 1998, we developed the first fully functional 3-D CZT spectrometer[4]. The 3-D position sensitivity of this CZT spectrometer using VA1 application specific integrated circuits (ASIC) chips enabled the correction for material non-uniformity and varying electron trapping. An energy resolution of 1.7% FWHM at 662 keV was achieved for single-pixel events from the whole bulk of a 1 cm^3 3-D CZT detector. However, the first-generation 3-D CZT spectrometer can only get the energy and 3D position information for single-pixel events.

After five years of efforts and a fruitful collaboration between our group and Ideas ASA[5], we introduced in 2003 the 2nd-generation 3-D CZT system using the VAS2/TAT2 ASIC[6]. With the ability of sensing the electron drift time for each individual interaction, these 2nd-generation 3-D CZT systems can get the energy and 3D position information for multiple-pixel events. Intelligent gamma-ray spectroscopy[7] and 4π Compton imaging[8] have been successfully implemented using these 2nd-generation 3-D CZT spectrometers.

However, several problems had been discovered. Firstly, the electronic noise was fairly high (~5-6 keV in different channels), limiting the energy resolution to 1.1% FWHM at 662 keV for single-pixel events. Secondly, the front-end board was not properly designed causing very large cross-talk on the cathode induced by digital control signals. This leads to high cathode triggering threshold (~100 keV). Thirdly, only one global threshold can be set for all the channels reading the signals from anode pixels. Because of the variations of the DC offsets in these channels, the global threshold has to be set above the highest threshold of all the channels, causing a fairly high triggering threshold in the

* Further author information: (Send correspondence to Feng Zhang)
E-mail: zhangf@engin.umich.edu

Hard X-Ray and Gamma-Ray Detector Physics VI, edited by Arnold Burger, Ralph B. James, Larry A. Franks, Proc. of SPIE Vol. 5540 (SPIE, Bellingham, WA, 2004) · 0277-786X/04/$15 · doi: 10.1117/12.563903

anode pixels (~80 keV). Lastly, significant non-linearity was observed in the VAS2 (energy) channel, increasing the complexity in the calibration and degrading the energy resolution for multiple-pixel events.

The 3rd-generation ASIC – VAS3.1/TAT3 has been designed to address the problems described above. This paper briefly introduces the basic system configuration of the 3rd-generation 3-D CZT spectrometers. The experimental results from one detector system are presented and discussed.

2. SYSTEM DESCRIPTION

A 3-D CZT spectrometer consists of a CdZnTe detector module with a ceramic substrate, an ASIC front-end board, and a controller (repeater) card (MCR3). The CdZnTe detector is wire-bonded to the ASIC inputs. The MCR3 repeater card is used to generate and send the readout clock signals to the ASIC and also convert the output of the ASIC to the voltage signal needed at the input of the data acquisition (DAQ) board. A PCI-6110 DAQ board from National Instruments is used as the A/D converter and as the controller interface between the DAQ program and the detector system.

2.1. Pixelated CdZnTe Detector Design

The detector, fabricated by eV-PRODUCTS[9], has an 11×11 pixelated anode and a planar cathode on a 1.5 × 1.5 × 1.0 cm^3 CZT crystal. The pixel pitch is 1.27 mm. There is a common grid between pixel anodes biased at negative voltage to focus the electrons to the pixel anodes. The trace width of the grid electrode is 100 μm with a 200 μm gap between the grid and the pixel. The anode pixel-grid pattern and the pictures of the detector are shown in Fig. 1(a)-(c).

Four VAS3.1/TAT3 chipsets are mounted on the front-end board to read out signals from 121 anode pixels and the cathode. The CZT crystal is mounted on a ceramic plate (cf. Fig. 1(c)). The conducting traces on the two sides of the ceramic plate connect every pixel anode to a corresponding metal pad on the periphery of the plate (cf. Fig. 1(b)). A short wire-bond connects each pad on the ceramic plate to the input of each ASIC channel on the front-end board (cf. Fig. 1(d)).

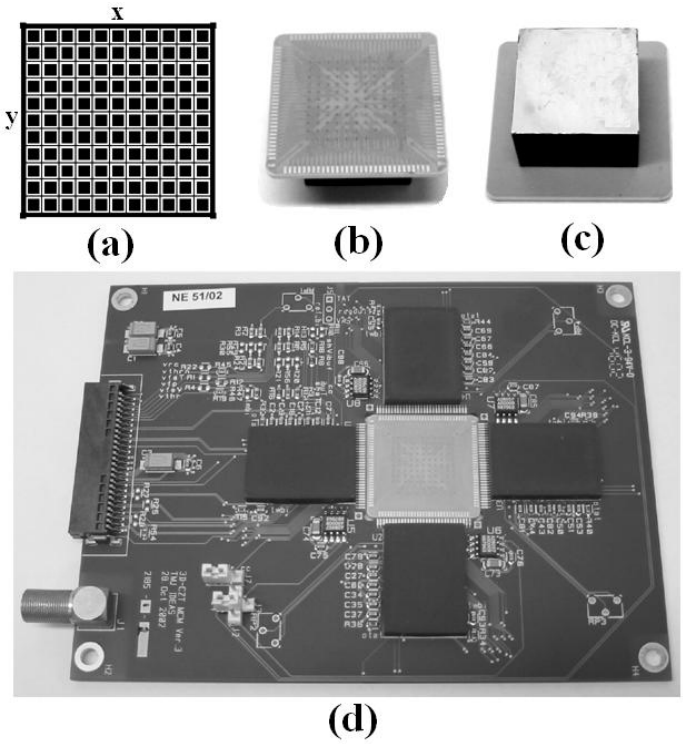

Figure 1. Pictures of the detector and the front-end board. (a). 11×11 anode pixel-grid pattern. (b). Photo of the detector with the ceramic substrate facing up. (c). Photo of the detector with the cathode facing up. (d). The ASIC front-end board with the CdZnTe detector placed in the center and wire-bonded to the ASIC inputs.

2.2. ASIC

The basic structure of the 3rd-general ASIC – VAS3.1/TAT3 is nearly the same as the VAS2/TAT2 ASIC. Several changes aiming to improve the system performance have been implemented in the VAS3.1/TAT3 ASIC. In the VAS2, because one channel (special channel) was used to readout the cathode signal (positive pulse) and the other channels (normal channels) were used to readout the anode signal (negative pulse), an inverter was added after the shaper in each normal channel to make anode signal polarity the same as the cathode polarity, so that all channels can employ a common design of peak-hold. However, the inverter is highly sensitive to temperature variation, causing the drifting of the baseline and the gain. This problem was solved with the use of two peak-hold circuits, one for anode signals and the other for the cathode signal, and the removal of the inverter. Another important improvement is that each channel now has a digital to analog converter (DAC) to fine-tune the low energy threshold. A more uniform triggering threshold can be achieved. Other minor changes, such as an additional test channel with the peak hold turned off, separate control of the preamp feedback resistance for the special channel and the normal channels, and the increase in the gain on TAT3 chips also help to diagnose the system response and improve system performance.

The VAS3.1 (version 3.1) ASIC chip is used to read out the induced charges on anode pixels and the cathode. The TAT3 (version 3) ASIC chip is used to trigger the system and read out the electron drift times. One VAS3.1 chip and one TAT3 chip form a chipset. The preamplifier output of each VAS3.1 channel is wire-bonded to the input of each TAT3 channel. Four chipsets are needed for each 121-pixel CZT detector.

Each VAS3.1 chip has 33 independent channels, each consisting of a preamplifier, a shaping amplifier, and a peak-hold and sample-hold circuit. The first channel on each VAS3.1 chip has an opposite polarity to the other 32 channels, to read out the signal from the cathode. Fig. 2 shows the basic structure of a single VAS3.1/TAT3 channel.

Each TAT3 chip also has 33 channels, each channel having a fast shaper, a discriminator for triggering and a timing to amplitude converter (TAC) for electron drift time sensing. A trigger mask can be set to disable those channels having high noise.

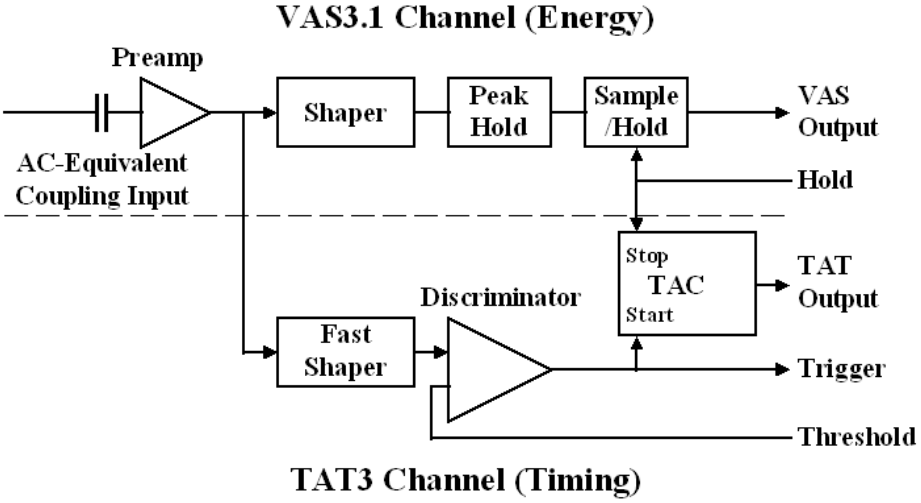

Figure 2. Illustration for the VAS3.1 (energy) and the TAT3 (timing) channels.

2.3. Depth sensing using C/A ratio and electron drift time

In the 3-D CZT spectrometer, the 2-D coordinates of interactions are determined from the individual location of the triggering pixels. For single-interaction events, because of the weighting potential, the cathode signal is proportional to both the deposited energy and the interaction depth, while the anode signal is almost proportional to the deposited energy. Thus, the interaction depth can be derived from the cathode to anode signal ratio[10]. However, for multiple-interaction events, we cannot obtain the depth for each individual interaction using the cathode to anode signal ratio. Instead, electron drift times for each triggering pixel are individually recorded. Assuming nearly constant electron drift speed inside the detector volume, the electron drift time can be used to obtain the depth for multiple-pixel events.

Fig. 3 illustrates the timing sequences of electron drift-time measurement for multiple-pixel events. When a gamma-ray interacts in the detector and the electron clouds start to drift, a trigger is generated by the TAT3 special channel when the induced signal on the cathode crosses a threshold. This trigger starts the TAC in the TAT3 special channel and generates the system trigger. When an electron cloud drifts near an anode pixel, the induced signal crosses a threshold, and triggers the corresponding TAT3 channel. This trigger starts the TAC in the TAT3 channel corresponding to that anode pixel. After a fixed delay after the system trigger, all the channels are held and read out in serial mode through a multiplexer built into the chips. By using peak-hold in addition to sample-hold circuits, the pulse amplitude of multiple-pixel events with different electron drift times (different peaking times) can be read correctly. The individual electron cloud drift times can be derived from the timing signal amplitudes generated by the TACs in the TAT3 channels.

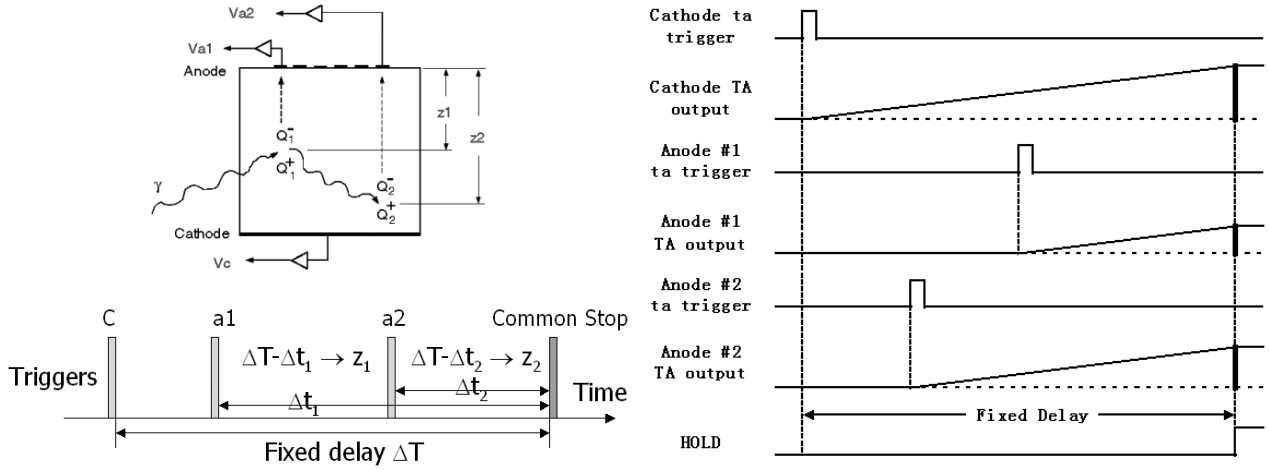

Figure 3. Interaction depth determination by electron drift time sensing. Vc is the signal from the cathode. Va1, Va2 are the signals from the anode pixel #1 and the anode pixel #2, respectively.

2.4. DAC thresholds

In the 2nd-generation system, the anode pixels have triggering thresholds ranging from 50 keV to 80 keV, with the spread caused by the variations of DC offsets and noise in each ASIC channel. However, only one global triggering threshold can be set for all the channels reading the anode pixels. As a result, the threshold has to set above the highest threshold among all channels (~80 keV). This problem has been solved in the new ASIC. In addition to the global threshold, a 4-bit DAC unit is added to each channel so that the threshold of each channel can be finely tuned to achieve more uniform thresholds among all the channels.

3. EXPERIMENTAL RESULTS AND DISCUSSION

One 3rd-generation 3-D CZT spectrometer was assembled and tested. The detector could be biased up to -2500 V on the cathode. But the cathode signal became unstable after several hours. Thus a lower bias of -2200 V was chosen as the cathode bias. Anode pixels were DC-coupled to the ASIC inputs and thus all at ground potential. The common grid electrode between the pixels was biased at a negative voltage to steer the electrons drifting towards the anode pixels. The larger the voltage difference between the anode pixels and the grid, the more efficient the steering effect is. However, we do not want the grid bias to be excessively high because high grid bias will result in high leakage current. By experiments, -60 V grid bias was finally chosen for reasonably low leakage current and high electron steering efficiency.

The whole system was operated at room temperature (~23℃). The detector was irradiated from the cathode side with uncollimated gamma-ray sources placed 5 cm away from the cathode. The ^{137}Cs 662 keV gamma-ray spectrum shown below was acquired over 40 hours. Spectra from ^{241}Am were also collected for measuring the electron mobility-lifetime products and estimating the electronic noise.

3.1. Improvements with the New Electronics

One problem of the 2nd-generation 3-D CZT system is that the baseline and the gain of the VAS2 ASIC are both very sensitive to temperature change. Although the baseline drift can be dynamically monitored and compensated by specifically designed DAQ program, and the gain drift can be calibrated for a range of environmental temperature, these temperature dependences still complicate the system calibration and degrade the energy resolution. This problem has been solved on the new VAS3.1 ASIC. Both the baseline and the gain are fairly stable in the 3rd-generation 3-D CZT system when the temperature varies by a few ℃ during the 40 hours data collection time.

Another limiting factor on the performance of the 2nd-generation 3-D CZT system is the large cross-talk induced on the cathode due to the improper layout of the digital signal traces on the front-end board. As a consequence, the triggering threshold of the cathode signal must be set above 100 keV otherwise the system will be retriggered continuously by the cross-talk. Since the anode pixels have much smaller area than the cathode, the induced cross-talk on the anode pixels is not so large but still not negligible. The triggering threshold of the anode signal ranges from 50 keV to 80 keV, varying from channel to channel due to the variations in DC offsets. Thanks to the newly designed front-end board in the 3rd-generation system, the cross-talk, although still exists, has been greatly reduced. As a result, the cathode triggering threshold has been lowered to ~50 keV and the anode triggering threshold has been lowered to ~25-35 keV.

3.2. Results for 662 keV Single-Pixel Events

With the help of 3D position sensing, the material non-uniformity, the weighting potential variations and the electron trapping variations can be corrected to the limit of the position resolution – estimated to be 1.27 mm × 1.27 mm × 0.2 mm. By doing 3-D corrections, an unprecedented energy resolution of 0.93% FWHM at 662 keV for single-pixel events has been achieved from the entire 2.25 cm^3 volume of the 3rd-generation 3-D CZT spectrometer, as shown in Fig. 4. As a result of the much lower thresholds than the previous systems, the 32 keV ^{137}Cs K x-ray has been observed in the 3-D CZT system for the first time.

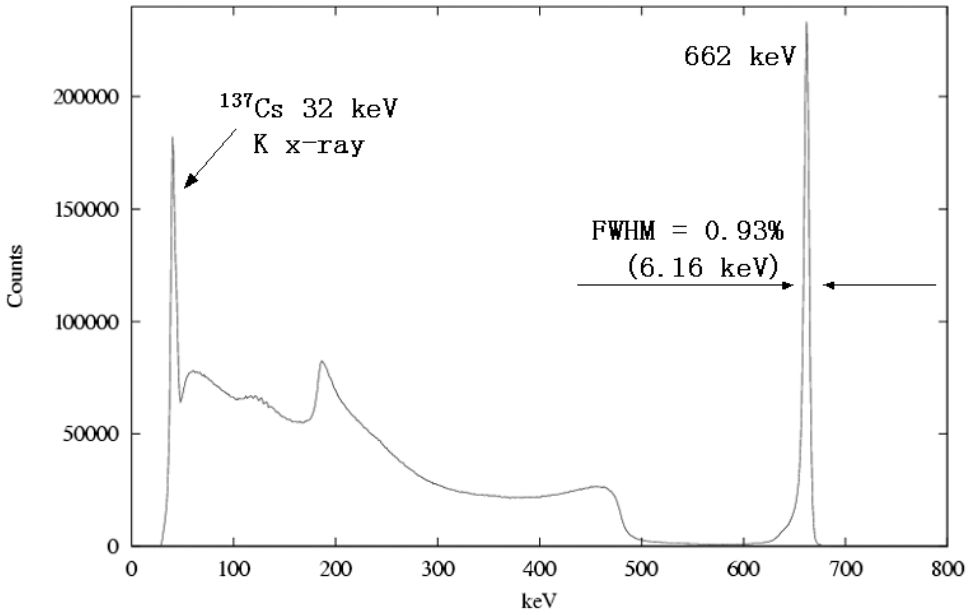

Figure 4. Energy spectrum of single-pixel events from an uncollimated ^{137}Cs source collected for 40 hours from all 120 working pixels.

Fig. 5 shows the energy resolution (FWHM at 662 keV) distribution for single-pixel events. The bad pixel in the lower-left corner of the detector map is probably due to bad wire-bond. We can see that more than 2/3 of the pixels have better than 1% FWHM energy resolution. If only these pixels with better than 1% resolution were selected (corresponding to ~1.5 cm^3 volume of CZT), an energy resolution of 0.86% FWHM at 662 keV was achieved.

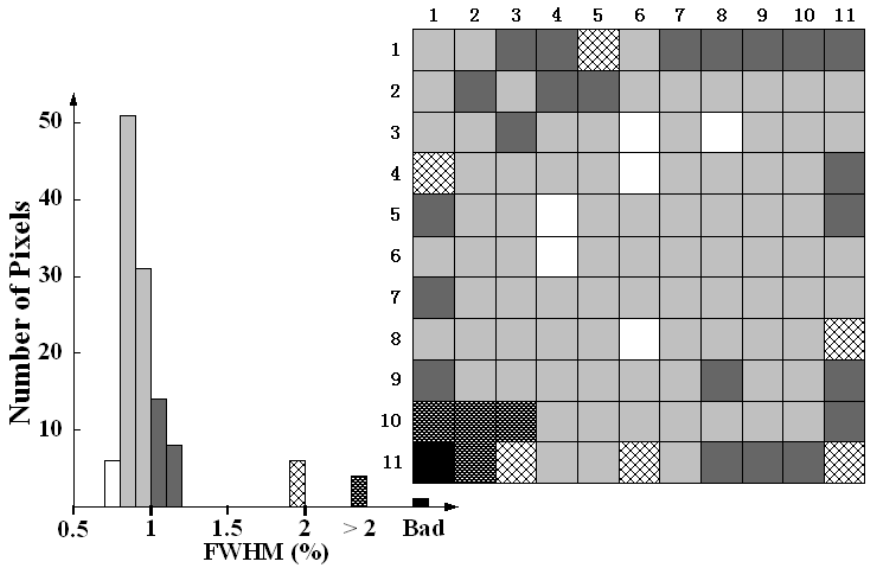

Figure 5. Energy resolution (FWHM at 662 keV) distribution for single-pixel events from an uncollimated ^{137}Cs source collected over 40 hours.

According to Ideas ASA's test report, the electronic noise in the ASIC is ~3 keV. However, due to a design limitation, the electronic noise of the ASIC cannot be directly measured after the ASIC has been wire-bonded to the detector. In order to estimate the overall electronic noise of the system, an uncollimated ^{241}Am source was placed 5 cm away from the cathode. The 59.5 keV gamma rays from the ^{241}Am source should all be stopped in a very thin layer on the cathode side. So, the collected anode signals should all come from the interactions at the same depth, without extra broadening due to depth dependence. The energy resolution of the ^{241}Am anode spectrum was measured to be ~4.8 keV FWHM. If we only consider the statistical fluctuation in the charge carrier creation and assume a Fano factor of 0.1, the electronic noise in the channels reading out the anode signal should be less than 4.5 keV FWHM after removing the photopeak broadening due to charge carrier generation from the observed overall energy resolution. Similarly, the electronic noise in the channel reading out the cathode signal was estimated to be ~7 keV FWHM.

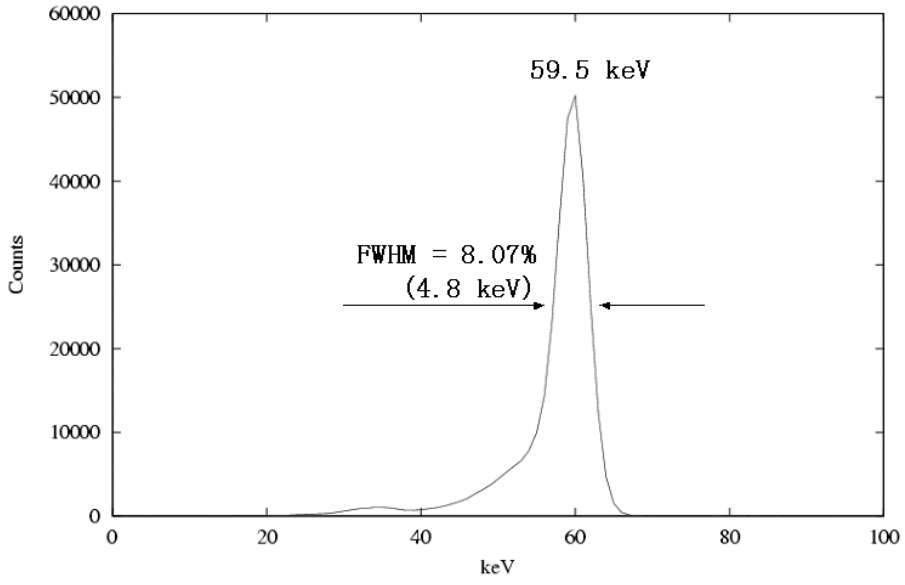

Figure 6. Energy spectrum for an uncollimated ^{241}Am source collected from all 120 working pixels.

3.3. Electron Mobility-Lifetime Product

The energy spectra of a ^{241}Am source irradiating from the cathode side were collected for each pixel under two different cathode biases, -1400 V and -2200 V. The electron mobility lifetime product can be estimated[11] using

$$(\mu\tau)_e = \frac{D^2}{\ln\left(\frac{H_{a1}}{H_{a2}}\right)}\left(\frac{1}{V_2}-\frac{1}{V_1}\right),$$

where D is the detector thickness, H_{a1} and H_{a2} are the photopeak centroids under two different cathode biases - V_1 and V_2. The measured $(\mu\tau)_e$ for all the pixels are shown in Fig. 7. No result can be calculated for two pixels in the lower-left of the map because of material defects.

1.87	2.38	2.35	2.73	2.68	2.19	2.38	2.37	2.47	2.80	2.55
2.53	2.33	2.06	2.36	2.20	2.34	2.38	2.67	2.46	2.58	2.66
2.77	2.74	2.60	2.08	2.75	2.75	2.40	2.48	3.05	2.67	2.63
2.50	2.33	2.63	2.11	2.36	2.28	2.79	2.69	2.78	2.92	2.46
2.67	2.35	2.65	2.13	2.66	2.77	2.82	2.98	2.89	2.85	2.54
2.70	2.72	2.35	2.34	2.34	2.75	2.38	2.78	2.84	2.82	2.43
2.35	2.66	2.42	2.79	2.42	2.79	2.87	2.87	2.62	2.93	2.79
2.44	2.71	2.28	2.73	2.38	2.75	2.90	2.53	3.05	2.91	2.94
2.46	2.28	2.36	2.33	2.36	2.39	2.87	2.47	3.06	3.07	2.89
0.00	2.00	2.21	2.64	2.37	2.89	2.42	2.54	2.98	3.01	2.63
0.00	0.00	2.03	2.18	2.69	2.72	2.28	2.80	2.49	2.60	2.56

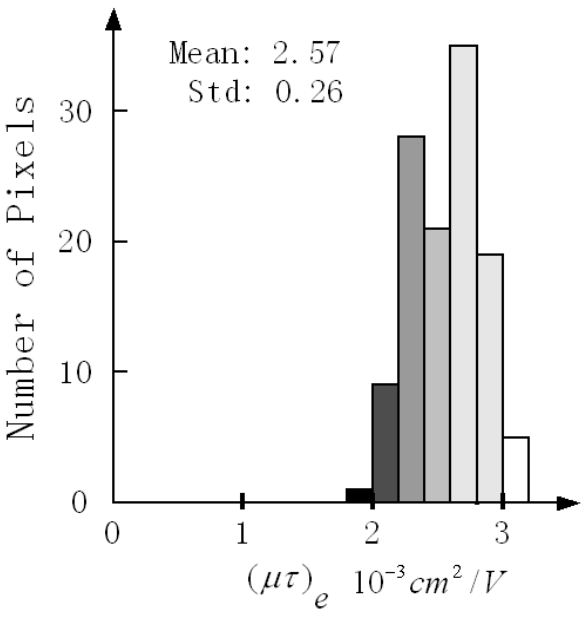

Figure 7. Calculated electron mobility-lifetime products (10^{-3} cm^2/V) for all working pixels. (Left): Pixel map of the $(\mu\tau)_e$ value, darker color corresponds to lower $(\mu\tau)_e$. (Right): Histogram of the $(\mu\tau)_e$ distribution for all working pixels.

3.4. 662 keV Two-pixel Events

For two-pixel events, the depth of each interaction can be derived from the electron drift time for each pixel. After the correction for timing-amplitude-walk, electron trapping and non-linearity for each signal, the true energy and 3-D position information can be obtained for each interaction. An energy resolution of 1.52% FWHM at 662 keV has been achieved for two pixel events collected from the entire volume of the detector, as shown in Fig. 8. When the 662 keV gamma ray interacts twice inside the detector volume, the probability of depositing all of the 662 keV energy is much higher than only one interaction. This is evident by comparing Fig. 4 and Fig. 8 as the peak to Compton ratio increases from ~9 to ~17. This feature can be very useful in applications where the peak to total ratio determines the measurement sensitivity.

Although an energy resolution of 0.93% FWHM at 662 keV has been achieved for single-pixel events, the energy resolution for two-pixel events was only 1.52% FWHM, worse than the conservatively estimated energy resolution based on single-pixel resolution – $\sqrt{(0.93\%)^2+(0.93\%)^2}=1.32\%$ FWHM. We can analyze the factors affecting the energy resolution for two-pixel events in more details.

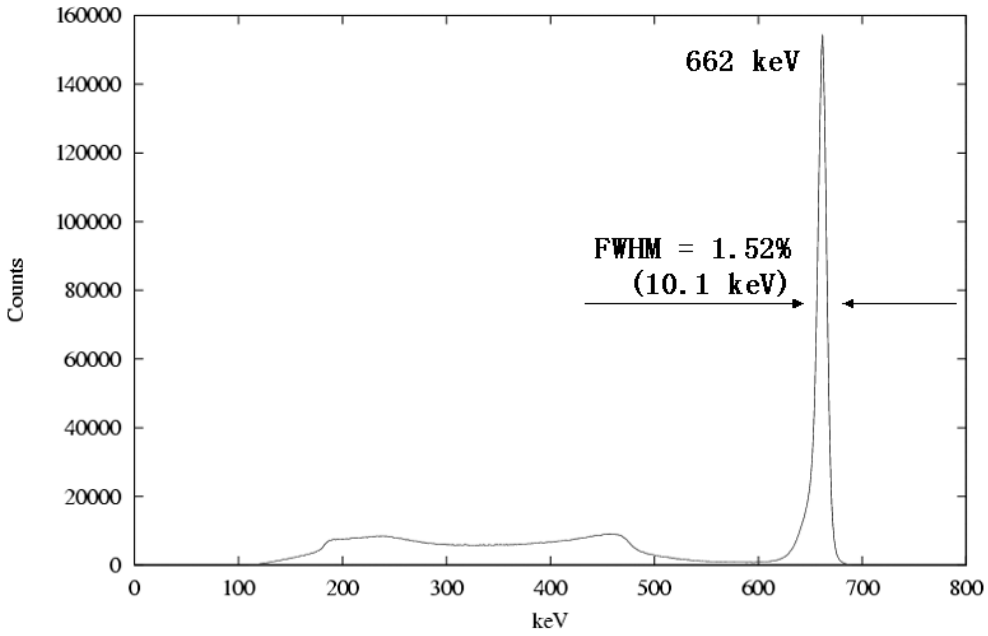

Figure 8. Energy spectrum of two-pixel events from an uncollimated ^{137}Cs source collected for 40 hours from all 120 working pixels.

First, we have estimated the electronic noise to be ~4.5 keV. The electronic noise from both pixels will contribute to the energy resolution degradation, at an estimated amplitude of $\sqrt{4.5^2 + 4.5^2} = 6.4$ keV by assuming that the noises are not correlated.

Secondly, due to the timing resolution of 15 ns FWHM, the depth resolution for two-pixel events is ~0.4 mm FWHM. So, the uncertainty in the depth will contribute an uncertainty of 4% to the depth correction. The total change of the photopeak centroids over the whole thickness (1 cm) of the detector is ~7%. Thus, this uncertainty is 4% × 7% × 662 keV = 1.86 keV.

Thirdly, the depth resolution for single-pixel events is ~0.2 mm FWHM and thus ~2% uncertainty in the depth correction – 2% × 7% × 662 keV = 0.93 keV. The contribution of factors other than the electronic noise and the depth uncertainty is $\sqrt{(0.93\% \times 662)^2 - 4.5^2 - 0.93^2} = 4.1$ keV.

Then, by adding all these known factors, we can get an estimation of the energy resolution for two-pixel events - $\sqrt{6.4^2 + 1.86^2 + 4.1^2} = 7.82$ keV FWHM or 1.2% FWHM. This is far better than the experimental result of 1.52% FWHM. There must be some other factors in an amount of $\sqrt{(1.52\% \times 662)^2 - 7.82^2} = 6.3$ keV FWHM contributing to the energy resolution degradation for two-pixel events. Possible factors, such as charge sharing, poor depth resolution at low energy, and non-linearity, are still under investigation.

4. FUTURE PLAN

So far, we have achieved our goal of better than 1% FWHM energy resolution at 662 keV for single-pixel events with our 3rd-generation 3-D CZT spectrometer. We are now investigating the reasons of the energy resolution degradation for multiple-pixel events. We plan to mount another 1.5 × 1.5 × 1 cm^3 CdZnTe detector with the new electronics. With the help of the excellent performance of the new system, by comparing the results from two systems, we hope to better understand the detector properties, such as material uniformity, defects, electron trapping, weighting potential and edge effects.

We are now collaborating with Ideas ASA to design the next generation 3-D CZT array system. The ASIC front-end board will be shrinked to the size of the detector and mounted on the anode side to form standard detector module.

Detector modules can be plugged on the motherboard to form a scalable array system. This will be an important step toward the application of the 3-D CZT systems in nuclear nonproliferation, homeland security, and space sciences.

5. CONCLUSION

With the help of the 3rd-generation ASIC – VAS3.1/TAT3, the performance of the 3D-CZT spectrometer has been greatly improved. The electronic noise is reduced to ~4.5 keV from ~6 keV of the previous ASIC. The triggering thresholds of the anode pixels are lowered to ~30 keV. By doing 3-D correction, an unprecedented energy resolution of 0.93% (6.16 keV) FWHM at 662 keV for single-pixel events has been achieved from the entire 2.25 cm^3 detector volume. The energy resolution for two-pixel events is 1.52% FWHM at 662 keV, worse than expected. The reasons for the energy degradation in two-pixel events are still under investigation. Future development of the 3-D CZT array system will have wide applications.

ACKNOWLEDGMENTS

This work was supported by the DOE/NNSA NA-22 office under Grant DE-FG03-01NN20122. We thank J.E. Berry of the College of Engineering for his work on detector mounting, A.B. Young of the Radiation Oncology Dept. and B.E. Casey of the Electrical Engineering and Computer Science Dept. at the University of Michigan for their work on wire-bonding.

REFERENCES

1. P.N. Luke, "Unipolar Charge Sensing with Coplanar Electrodes-Application to Semiconductor Detectors," *IEEE Trans. Nucl. Sci.* **42**, no. 4, pp. 207-213, Aug. 1995.
2. F.P. Doty, H.B. Barber, F.L. Augustine, J.F. Butler, B.A. Apotovsky, E.T. Young and W. Hamilton, "Pixelated CdZnTe detector arrays," *Nucl. Instrum. Methods A* **353**, pp. 356-360, 1994.
3. Z. He, W. Li, G.F. Knoll, D.K. Wehe, J.E. Berry, C.M. Stahle, "3-D position sensitive CdZnTe gamma-ray spectrometers," *Nucl. Instrum. Methods A* **422**, pp. 173-178, 1999.
4. W. Li, Z. He, G.F. Knoll, D.K. Wehe, J.E. Berry, "A Data Acquisition and Processing System for 3-D Position Sensitive CZT Gamma-ray Spectrometers," *IEEE Trans. Nucl. Sci.* **46**, no. 6, pp. 1989-1994, Dec. 1999.
5. Ideas ASA, Martin Linges vei 25, Snarøya, Norway.
6. F. Zhang, Z. He, D. Xu, G.F. Knoll, D.K. Wehe, J.E.Berry, "Improved Resolution for 3D Position Sensitive CdZnTe Spectrometers," *IEEE Trans. Nucl. Sci.*, to be published.
7. C.E. Lehner, Z. He, G.F. Knoll, "Intelligent Gamma-Ray Spectroscopy Using 3-D Position-Sensitive Detectors," *IEEE Trans. Nucl. Sci.* **50**, no. 4, pp. 1090-1097, Aug. 2003.
8. C.E. Lehner, Z. He, F. Zhang, "4 π Compton Imaging Using a 3-D Position-Sensitive CdZnTe Detector via Weighted List-Mode Maximum Likelihood," *IEEE Trans. Nucl. Sci.*, to be published.
9. eV-PRODUCTS, 375 Saxonburg Boulevard, Saxonburg, PA 16056, USA.
10. W. Li, Z. He, G.F. Knoll, D.K. Wehe, Y.F. Du, "A Modeling Method to Calibrate the Interaction Depth in 3-D Position Sensitive CdZnTe Gamma-Ray Spectrometers," *IEEE Trans. Nucl. Sci.* **47**, no. 3, pp. 890-894, Jun. 2000.
11. Z. He, G.F. Knoll, D.K. Wehe, "Direct measurement of product of the electron mobility and mean free drift time of CdZnTe semiconductors using position sensitive single polarity charge sensing detectors," *J. Appl. Phys.*, **84** (10)(1998) 5566.